LA-UR-18-27325
Approved for public release; distribution is unlimited.

Title: PAGOSA Simulations for the LANL Blast Tube

Author(s): Hughes, Justin Matthew
Terrones, Guillermo

Intended for: Report

Issued: 2018-08-01

PAGOSA Simulations for the LANL Blast Tube

Justin M. Hughes
Guillermo Terrones
X-Theoretical Design, Safety and Surety (XTD-SS)

Abstract

A parameter study was performed for the Los Alamos National Laboratory Blast Tube to tune geometry to best replicate peak blast pressures from experiments. Charge placement, reflecting wall thickness, flange gap width, and reflecting wall stand-off were sampled using a Latin-Hypercube design to train a Radial Basis Function Network surrogate model. This surrogate model was then used with a Nelder-Mead Simplex minimization routine to minimize error for the surrogate predictions.

1. Introduction

The LANL blast tube is used to generate directed blast waves to test blast effects on full scale test articles. The tube consists of five 30 ft long sections with an 8 ft outer diameter and 2 in wall thickness bolted together at standard pipe flanges and is made from A36 steel. The closed end is a reinforced rail cart with a large, free-floating steel plate acting as a shock reflector. An explosive is placed a set distance from the reflecting wall and test articles are placed at the open end of the tube. Figure 1 shows an aerial view of the tube at the test site before modification of the rail cart. This report summarizes simulation and research efforts to match experimental pressure pulses with the PAGOSA hydrocode [1]. In terms of dimensions and geometric extent, the blast tube is the largest geometry modeled in PAGOSA.

A parameter study was carried out to investigate the variation of the charge position relative to the reflecting wall, reflecting wall thickness, and flange gap width and their effect on peak pressure. This was accomplished by following the statistical method of Latin-Hypercube sampling [2]. Python was used to generate the PAGOSA input files with the varying parameters. A Radial Basis Function Network (RBFN) [3] surrogate model was used with a Nelder-Mead simplex minimization routine [4] from the SciPy Optimize module [5] to find the minimum error solution for a simple sum of the errors cost function of the peak gauge pressure at the end of the blast tube for two experiments where the amount of the C4 explosive was varied, BTC-08 (75 lbs of C4) and BTC-10 (115 lbs of C4) which used similar charge setups and data acquisition methods.

Figure 1. Aerial view of the LANL Blast Tube

2. Methods

2.1 Parameter Space and Sampling

The parameter space for this optimization problem was constrained to relevant geometry rather than changing the equation of state tuning for the C4. Table 1 shows the geometry variables used for the simulations and their respective sampled ranges. A total of 20 Latin-Hypercube samples with 2 extremal value samples was used to explore the input space.

Table 1. Parameter Space for Geometry Optimization

Parameter	Minimum	Maximum
Reflector Gap (in)	0.5	5
Reflector Thickness (in)	0.25	1.5
Charge position (ft)	9.5	10.5
Flange Gap (in)	0.004	0.4

2.2 Radial Basis Function Network (RBFN) surrogate model

A Radial Basis Function Network (RBFN) python class variable was created to emulate simulation data. The RBFN surrogate uses radial basis functions to calculate the weight of influence of a given dataset. The output of the RBFN is then the linear combination of these weights. The network can be described using the equation:

$$f(\boldsymbol{x}) = \sum_{i=1}^{n} w_i \varphi(\|\boldsymbol{x} - \boldsymbol{c_i}\|) \tag{1}$$

where $f(\boldsymbol{x})$ is the function being approximated, w_i is the network of weight factors, $\boldsymbol{x}$ is the vector of model inputs, and $\boldsymbol{c_i}$ are the set of N training points sampled from the input space. The function $\varphi(\|\boldsymbol{x} - \boldsymbol{c_i}\|)$ is a radial basis function applied to the distance between the test point $\boldsymbol{x}$

and the training points $\boldsymbol{c_i}$. Common basis functions are Thin Plate, Gaussian, Multiquadric, and Inverse Multiquadric. Much like shape functions used in finite element methods, these basis functions control the weight of the interpolations between the $\boldsymbol{c_i}$ training points at each test point of interest. The quantity $\|\boldsymbol{x} - \boldsymbol{c_i}\|$ is the Euclidean distance between the test point and each training point; that is, the radius between the N-dimensional points. Functional forms for these common basis functions are as follows:

$$\varphi(\|\boldsymbol{x} - \boldsymbol{c_i}\|) = \varphi(r) = r^2 \ln(\mathrm{kr}) \quad \text{(Thin Plate)} \tag{2}$$

$$\varphi(\|\boldsymbol{x} - \boldsymbol{c_i}\|) = \varphi(r) = \exp(kr^2) \quad \text{(Gaussian)} \tag{3}$$

$$\varphi(\|\boldsymbol{x} - \boldsymbol{c_i}\|) = \varphi(r) = \sqrt{r^2 - k^2} \quad \text{(Multiquadric)} \tag{4}$$

$$\varphi(\|\boldsymbol{x} - \boldsymbol{c_i}\|) = \varphi(r) = \frac{1}{\sqrt{r^2 - k^2}} \quad \text{(Inverse Multiquadric)} \tag{5}$$

where the constant *k* is a tuning parameter which can be changed increase accuracy of the surrogate. Of the 22 samples taken, 4 were reserved for model validation. The SciPy optimization routine (scipy.optimize.minimize) is used to obtain a suitable tuning parameter within the RBFN class my minimizing the validation error of reserved data sets.

3. Results and Discussions

Simulations were performed with the finite-difference hydrocode PAGOSA with a 1 cm mesh resolution in a 302x6334 cell grid on 576 processors with an average run time of 8.5 hours. The end tube pressure data was read from a tracer near the tube wall 5 ft from the open end of the tube. Stress data for each charge configuration was read from the outside of the tube wall at the charge centerline. The geometry of the initial model is shown in Figure 2. The materials and models used are described in Table 1. Here, the roll cart is modeled as a large cylindrical steel mass.

The C4 charge is modeled as a hollow cylinder with an inner diameter of 1.65 in. The carbon fiber backbone of the charge was modeled as a Poly(methyl methacrylate) (PMMA) plastic cylinder. This cylinder provides confinement for the interior of the charge and prevents the Jones-Wilkins-Lee equation of state for the C4 charge from becoming overdriven due to reflected shocks from the axisymmetric mesh boundary. For BTC-8, the 75 lb charge was approximately 50 in long, giving a linear weight density (LWD) of 18 lb/ft. For the hollow charge geometry, this gives and outside diameter of 5.3929 in to match the LWD of the experiment. For simplicity, both the 75 lb and 115 lb simulations use the same charge diameters. The actual LWD for BTC-10 was approximately 14.375 lb/ft with a 115 lb charge about 96 in long.

The initial model for the A36 tube was a solid-walled hollow cylinder ignoring gaps at the bolted flanges. Due to overpredictions of pressure at nearly every charge weight, extra energy losses were required. The flanges were later inserted and modeled as a simple gap at the end of the tube sections every 30 ft. However, after performing a preliminary study on the tube geometry by taking Latin-Hypercube samples of the reflecting wall thickness (0.25 - 1.5 in),

flange gap width (0.004 - 0.4 in), charge position relative to the closed end (9.5 - 10.5 ft), and the reflecting wall gap with the tube (0.5 – 5.0 in), the optimized RBFN surrogate model was unable to predict pressures for subsequent PAGOSA runs for the 115 pound charge weight and simulations would be consistently >20 psi high. Instead of increasing the flange gap width, more flange gaps were inserted along the length of the tube every 15 ft to allow for bleeding off more energy. Doing so enabled the RBFN to optimize within ~3 psi of both 75 lb and 115 lb PAGOSA simulations for the same geometry. Both surrogates were trained on 18 samples, with the remaining 4 used as validation sets for the RBFN tuning parameter (k in equations 2-5). For this sample, the optimized geometry was mostly stable with respect to the number of training sets versus validation sets.

Air was given the highest priority for the PAGOSA advection algorithm for the initial geometry study. Typically, simulation material priorities are in the order of the expansion of the HE in the direction of material flow (e.g. booster > HE > confinement > air > steel). The entire study was repeated using material priorities in the order of expansion for flow to the right for two cases: flange gaps every 30 ft and flange gaps every 15 ft. For both cases, the RBFN was unable to predict PAGOSA output for any optimized geometry. An additional 28 samples (50 total samples) were taken for each charge weight to provide more data for the RBFN to discern parameter relationships. Even with the additional samples, the RBFN surrogate was unable to predict PAGOSA simulation output. Additionally, the surrogate demonstrated a wildly variable optimized solution depending on the number of datasets trained on for the new priority order. From this it was decided to stick to the initial material priority order.

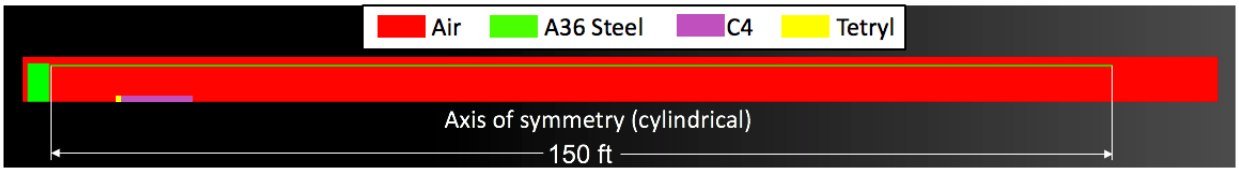

Figure 2. Blast tube geometry in PAGOSA (charge size exaggerated)

Table 1. Materials and models for PAGOSA simulations

Material	Equation of State	Strength	Burn	Priority
A36 Steel [6,7]	Mie-Gruneisen	Johnson-Cook	-	2
C4	Jones-Wilkins-Lee	-	Programmed	4
Tetryl	Jones-Wilkins-Lee	-	Programmed	5
Air	SESAME (5030)	-	-	1
PMMA	SESAME (7750)	Elastic-Perfectly Plastic	-	3

3.1 Shock Front Time-of-Arrival

In order to extract time-of-arrival (TOA) data for the shock front in PAGOSA, artificial viscosity for air is monitored using tracer particles near the tube wall. The first peak in artificial viscosity is associated with shock traversal in air before the reaction product gases reach the tracers. Figure 3 shows the TOA for a PAGOSA simulation of a 75-pound C4 shot compared to experiments using a hollow charge geometry with varying types of confinement. For these

simulations, having no confinement, especially for the interior of the charge, causes the Jones-Wilkins-Lee (JWL) equation-of-state (EOS) to become overdriven. Having exterior confinement causes the shock propagation to slow down. For all simulations hereafter, hollow charge configurations will use an interior confinement of low density PMMA (~0.6 g/cc) with a SESAME EOS to hinder interior shock reflections.

3.2 Effect of Charge Diameter on Tube Stresses

An early investigation was to determine the effect of the charge setup, namely the diameter of the charge, on stresses in the tube. For constant weight, changing the outer diameter changes the linear weight density (LWD) which directly influences the amount of explosive burned per foot of charge. Figure 4 shows the effect of changing the LWD for the 75 pound and 115 pound shots.

The peak pressure readouts for both the 75 lb and 115 lb C4 simulations show a more or less undefined relationship for change in pressure versus a change in linear weight density but overall show a general increase as linear weight density increases. Both peak stresses and peak total- and plastic deflection values directly follow the increase in linear weight density.

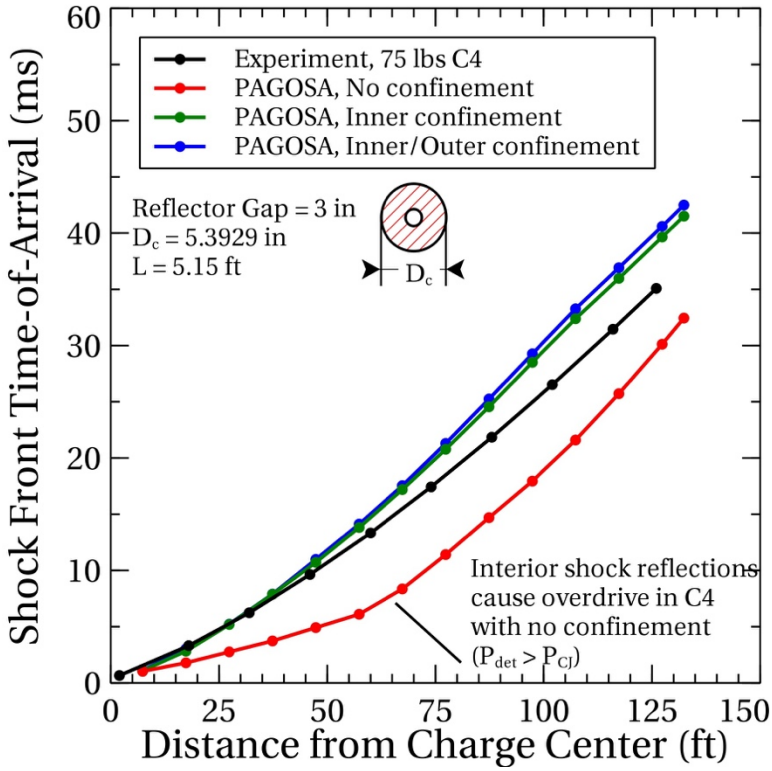

Figure 3. Time-of-arrival (TOA) data for 75 pounds of C4 with varying methods of confinement

3.3 Optimizing Pressure Pulse Curves

As a first pass at optimizing the problem geometry and replicating experimental values, the entire pressure pulse curves were used as an optimization target. To improve model correlations

to experimental data and reduce signal noise, the experimental data signals were filtered using a Savitsky-Golay filter, interpolated to the same timesteps, and averaged. Figure 5 gives an example of a Savitsky-Golay filtered dataset for the BTC-8 experiment. Due to late time error buildup at the far-right transmissive mesh boundary, a large pressure builds on the mesh and subsequently shoots back down the tube in the opposite direction, typically twice the outgoing pressure. As a consequence, experimental and simulation signals are cut off at 60 ms.

Due to the high variability of the shock wave timing down the tube due to changes in geometry, the simulated shock front lags between 3 ms to 6 ms behind. This causes the surrogate model prediction of the initial pressure jump to fall well below expected. In order to best match pressure curve shape, the timing for each simulation is adjusted such that the maximum pressure occurs at the same time as the experiment's max pressure. A secondary surrogate model is then used to predict the lag time of the simulation. Figure *6a* shows the minimum error surrogate prediction compared to the experimental data for BTC-8. For figure 6a, the experimental and simulation curves were downsampled to 190 points from the approximately 40,000 experimental curve samples to reduce computational time of the optimization routine. Figure *6b* shows a comparison of the optimized surrogate with a PAGOSA simulation using the optimized constants. The bounding from the model is a 95% probability range that results from a 5% perturbation of all variables with a Monte Carlo Simple Random Sampling (MCSRS) routine mainly to check model robustness around the optimized point.

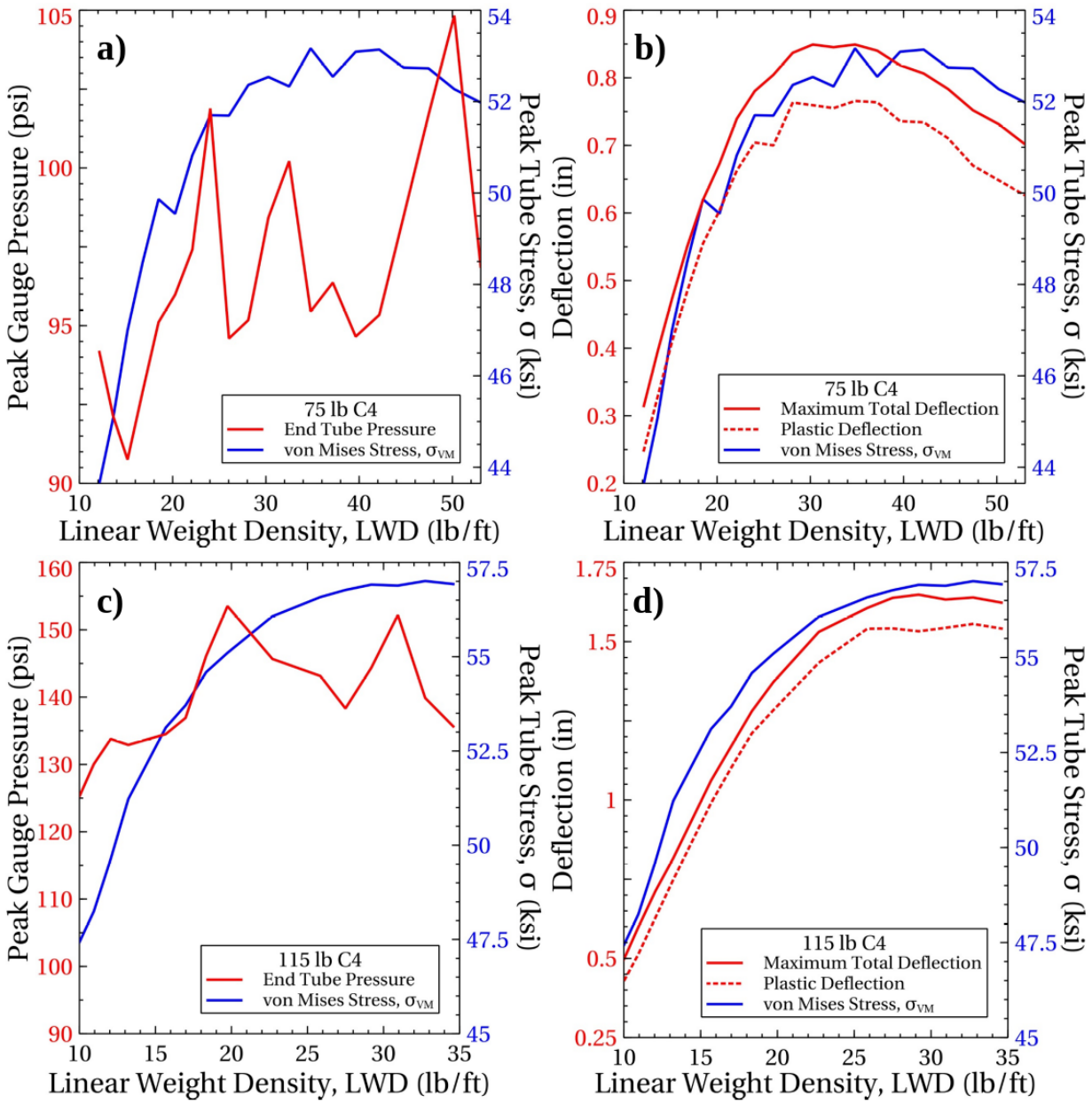

Figure 4. Effect of Linear Weight Density (LWD) for charges of constant weight showing a) peak pressure and stress for 75 lbs of C4, b) maximum deflection and stress for 75 lbs of C4, c) peak pressure and stress for 115 lbs of C4, and d) maximum deflection and stress for 115 lbs of C4

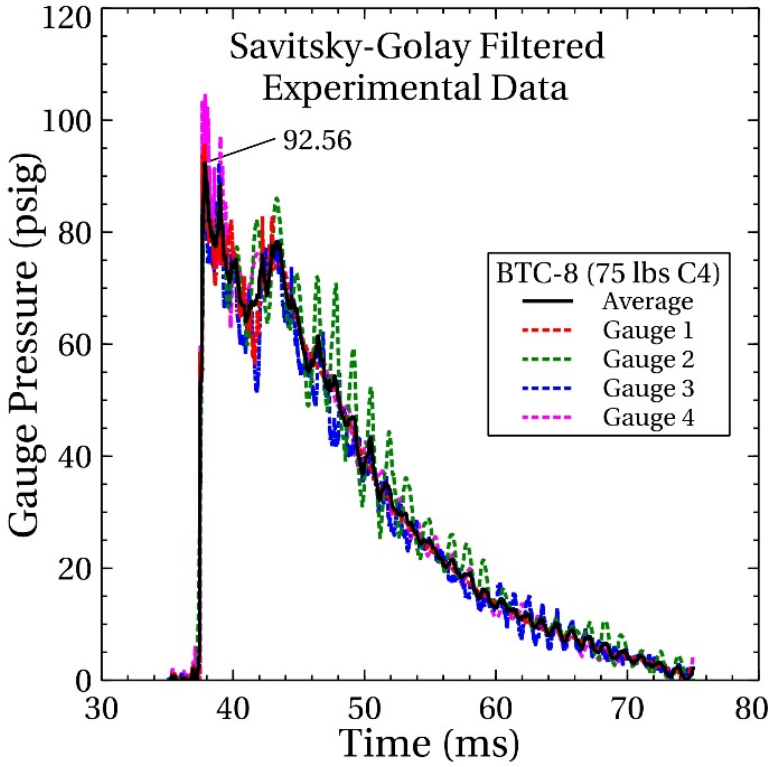

Figure 5. Averaged gauge pressure data signals for shot BTC-8

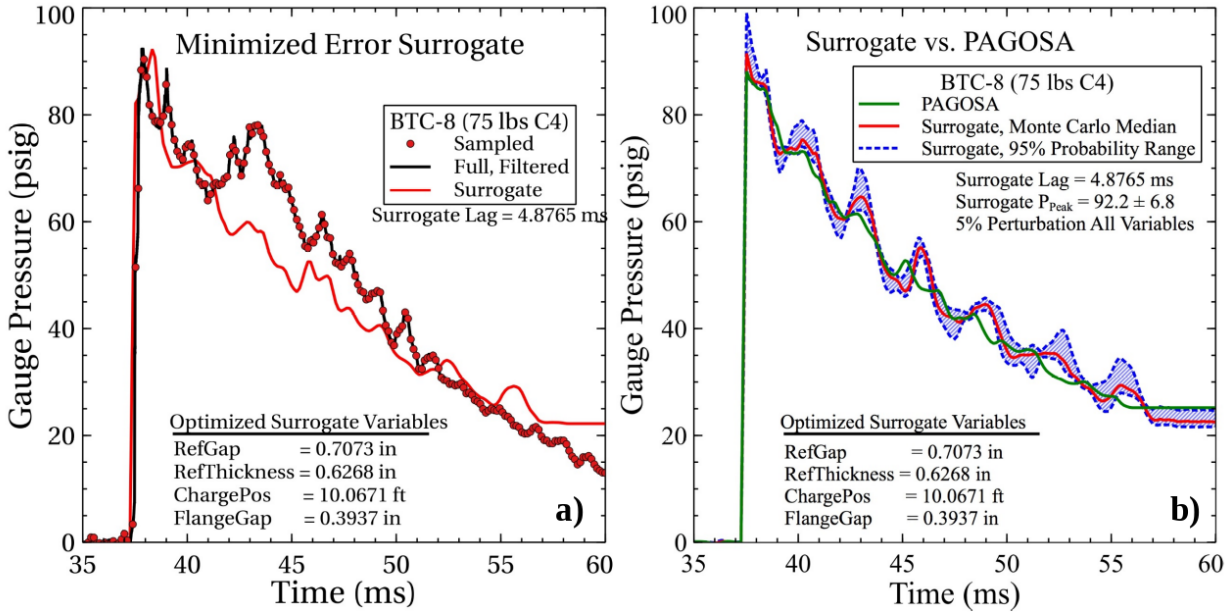

Figure 6. a) Surrogate model best fit using the Nelder-Mead simplex method and b) comparison of optimized surrogate model with PAGOSA results for optimized constants

Using the constants optimized from the 75 lb of C4 shot, a 115 lb of C4 simulation was performed. This resulted in a significant overprediction in peak pressure as shown in Figure 7. By tuning the system to best represent BTC-8, the peak pressure for higher weight charges is overestimated. The inverse in true when tuning to BTC-10; peak pressures for lower charge

weights are significantly underpredicted. Two surrogate models were then trained for the 75 lb and 115 lb simulations separately and a simple sum of the errors cost function was used to minimize the error for both surrogates. However, when testing the optimized geometry from the multi-objective optimization for the 115 pound simulation, the PAGOSA results were not within an acceptable range of the surrogate model. The surrogate model would optimize to ~120 psig for peak pressure whereas the PAGOSA run for the same constants would predict ~150 psig for peak pressure. Though this problem may have been solved by taking more curve samples (significantly increasing optimization run times), it was decided to optimize the geometry using the peak pressure values only and disregarding timing.

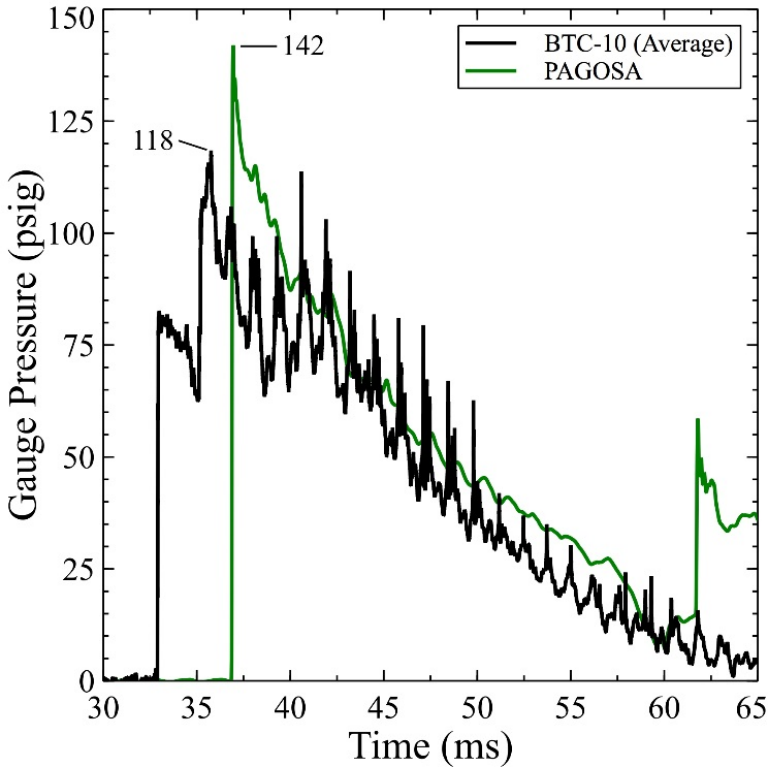

Figure 7. 115 lb C4 PAGOSA simulation using constants optimized from 75 lb C4 surrogate model

3.4 Optimizing to Peak Pressures

Since optimizing the surrogate models to the full pressure pulse misses the peak pressure for the 115 lb C4 simulations, the surrogate model and optimization scheme was used to emulate peak pressures only. The same multi-objective cost function, the simple sum of the errors for 75 lb and 115 lb simulations, was used. A multitude of optimization objectives were tested. Table 2 shows the optimization targets and their resulting model geometries and predicted PAGOSA outputs. Figure 8 shows the PAGOSA results using the RBFN optimized constants for both 75 lb and 115 lb charge weights. Since both charges have the same linear weight density, tube deflections should be nearly identical. Figure 9 shows the tube deflections for both the 75 lb and 115 lb simulations.

Table 2. Blast tube simulation geometry resulting from varying optimization targets

					75 lb C4		115 lb C4	
Optimization Target	**Reflector Gap (in)**	**Reflector Thickness (in)**	**Charge Position (ft)**	**Flange Gap (in)**	**Max Gauge Pressure (psi)**	**Max von Mises Stress (ksi)**	**Max Gauge Pressure (psi)**	**Max von Mises Stress (ksi)**
75 lb Minimum Stress	0.6919	0.7923	10.4130	0.0039	87.4511	44.3962	124.7950	49.4782
115 lb Minimum Stress	1.4111	0.6471	9.7603	0.1382	85.7134	46.5068	129.3642	44.1558
BTC-8 Peak Pressure	0.6489	0.5476	10.2494	0.3170	92.5573	47.1097	128.4351	47.3449
BTC-10 Peak Pressure	0.6748	0.4969	9.9382	0.3913	92.2577	46.5282	118.4522	47.5546
BTC-8/10 Peak Pressure	0.6488	0.6043	9.9054	0.3919	92.5573	46.4849	118.4522	47.1020

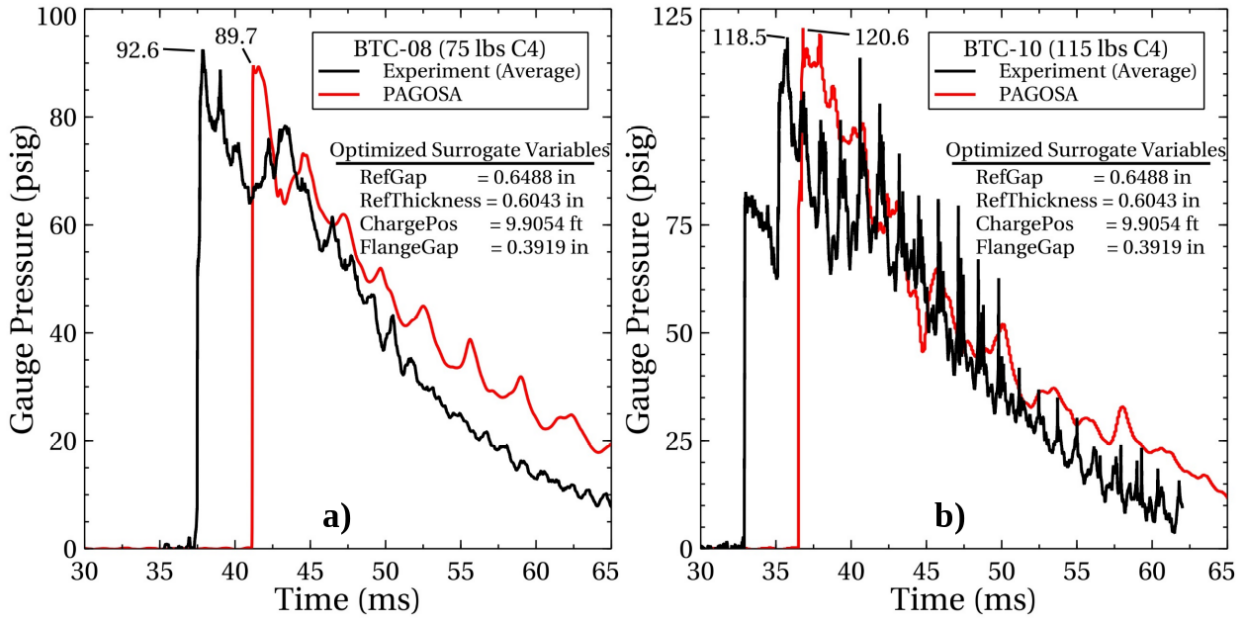

Figure 8. PAGOSA simulations for multi-objective optimized surrogates for a) 75 lbs C4 and b) 115 lbs C4

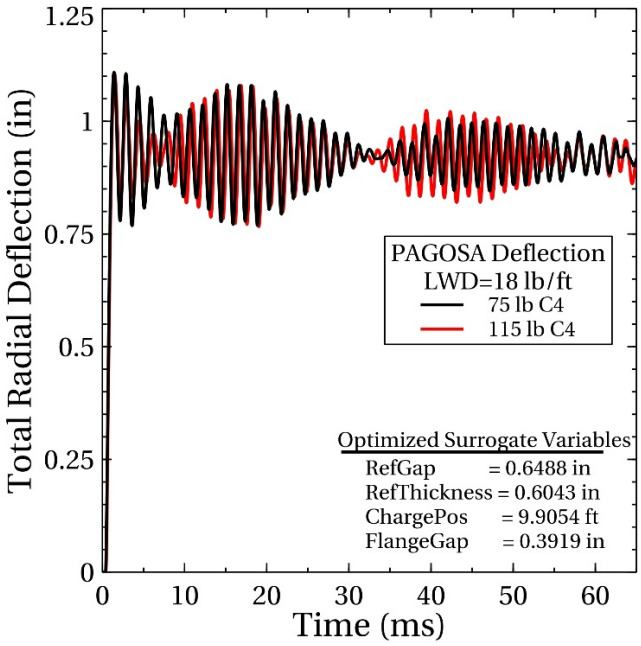

Figure 9. Tube deflection versus time for 75 lb and 115 lb C4 simulations

3.5 Charge Weight Study

After optimizing the simulation geometry to best reproduce BTC-8 and BTC-10 (75 lbs and 115 lbs, respectively) an additional check was made to check for pressure drop-off for higher weight charges. From experiments with other explosives in the blast tube, pressure would begin dropping off after a specific weight instead of the gradual, near-linear increase that's expected. Before optimization, PAGOSA predictions showed a near-linear increase in peak pressure with increasing charge weight. Figure 10 shows the behavior of the end tube peak pressure as a function of charge weight. Each charge used the same hollow tube geometry with the same linear weight density (18 lb/ft).

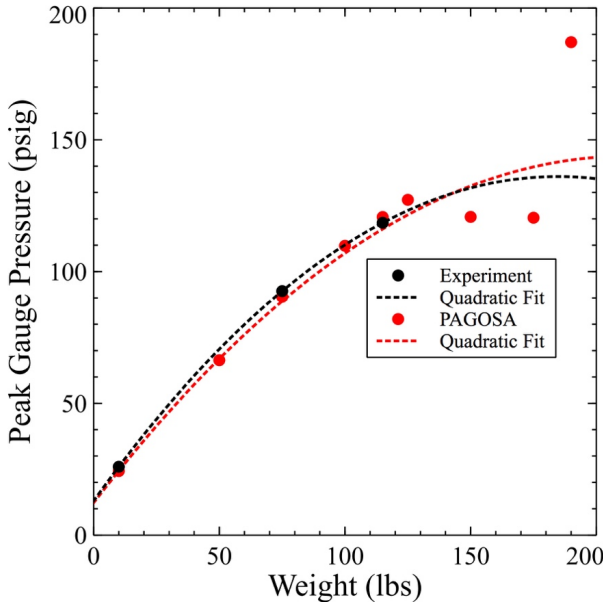

Figure 10. End tube peak pressure versus charge weight for experiment and PAGOSA simulations using geometry optimized to BTC-8 and BTC-10

For the optimized geometry, the peak pressure delivered to the open end of the tube drops off after 125 lbs with a sudden spike at 190 lbs of C4. The pressure trace changes dramatically at this point as shown in Figure 11. Above 115 lbs of C4, the pressure pulse becomes less definite and the incident shock front fails to form a planar shock front. The incident shock from the hollow center of the charge entrains a "jet" of gas products as the charge detonates. Above 115 pounds, this gas jet carries a shock at the tip. Subsequent radially reflected shocks from the tube wall interrupt the formation of the planar shock front.

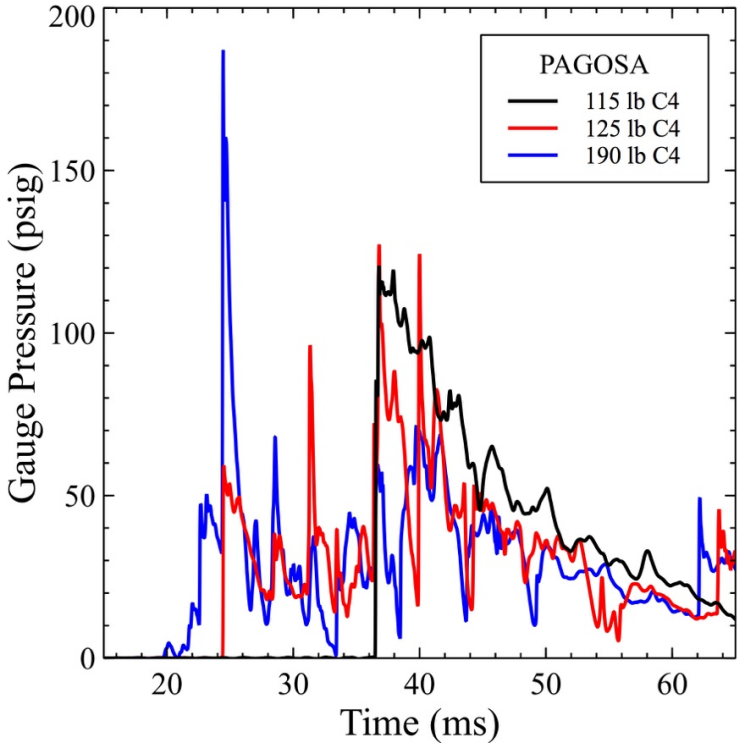

Figure 11. PAGOSA End tube pressure pulse for 115, 125, and 190 lbs of C4

4. Conclusions

The following are conclusions and potential future improvements of this study:

- PAGOSA was able to replicate two experimental data points for 75 and 115 pounds of C4. However, the geometry required is not the as-built blast tube geometry (flanges every 15 ft). Further investigation into the SESAME for air is encouraged.
- The late-time difference in time-of-arrival may be improved by using a smaller mesh size, though at a significant detriment to simulation run time due to the size of the problem. Improvements in energy delivery may be made by using a smaller mesh size around the HE charge while maintaining the large mesh size towards the open end of the tube.
- A Radial Basis Function Network (RBFN) was capable of predicting PAGOSA output within a reasonable level of accuracy (within 3 psi) using just the pressure

pulse peak values. Optimizing geometry using downsampled pressure pulse curves gave too much weight to the pressure drop-off which would cause the surrogate to miss the peak pressure.

5. References

[1] W. N. Weseloh, Clancy, S. P., Painter, J. W., PAGOSA Physics Manual, Los Alamos National Laboratory, Report LAUR-14425- M, 2010.

[2] M. D. McKay, Beckman, R. J., Conover, W.J., "Comparison of three methods for selecting values of input variables in the analysis of output from a computer code," *Technometrics*, 21:2, 239-245, 1979.

[3] D. Buhmann, M. (2003). Radial basis functions: Theory and implementations. Radial Basis Functions. 12. 10.1017/CBO9780511543241.

[4] Nelder, J A, and R Mead. 1965. A Simplex Method for Function Minimization. The Computer Journal 7: 308-13.

[5] Jones E, Oliphant E, Peterson P, *et al.* **SciPy: Open Source Scientific Tools for Python**, 2001-, http://www.scipy.org/

[6] Seidt, J.D., Gilat, A., Klein, J.A., Leach, J.R., "High Strain Rate, High Temperature Constitutive and Failure Models for EOD Impact Scenarios," Proceedings of the SEM Annual Conference & Exposition on Experimental and Applied Mechanics, Society for Experimental Mechanics, 2007.

[7] Roy, S.K., Trabia, M., O'Toole, B., Hixson, R., Becker, S., Pena, M., Jennings, R., Somasoundaram, D., Matthes, M., Daykin, E, Machorro, E., "Study of Hypervelocity Projectile Impact on Thick Metal Plates," *Shock and Vibration*, V2016, Article ID 4313480, 11p, 2016. https://doi.org/10.1155/2016/4313480